Bulletin of the Seismological Society of America. Vol. 67, No. 6, pp. 1529–1540. December 1977

ABSORBING BOUNDARY CONDITIONS FOR ACOUSTIC AND ELASTIC WAVE EQUATIONS

By Robert Clayton and Björn Engquist

ABSTRACT

Boundary conditions are derived for numerical wave simulation that minimize artificial reflections from the edges of the domain of computation. In this way acoustic and elastic wave propagation in a limited area can be efficiently used to describe physical behavior in an unbounded domain. The boundary conditions are based on paraxial approximations of the scalar and elastic wave equations. They are computationally inexpensive and simple to apply, and they reduce reflections over a wide range of incident angles.

Introduction

One of the persistent problems in the numerical simulation of wave phenomena is the artificial reflections that are introduced by the edge of the computational grid. These reflections, which eventually propagate inward, mask the true solution of the problem in an infinite medium. Hence, it is of interest to develop boundary conditions that make the perimeter of the grid "transparent" to outward-moving waves; otherwise a much greater number of mesh points would be required.

One solution to the problem that has been proposed (Lysmer and Kuhlemeyer, 1969) is the viscous damping of normal and shear stress components along the boundary. This method approximately attenuates the reflected compressional waves over a wide range of incident angles to the boundary, but it does not diminish reflected shear waves as completely. Another method that can be made to work perfectly for all incident angles has been proposed by Smith (1974). With this approach, the simulation is done twice for each absorbing boundary: once with Dirichlet boundary conditions, and once with Neumann boundary conditions. Since these two boundary conditions produce reflections that are opposite in sign, the sum of the two cases will cancel the reflections. The chief shortcoming of this method is that the entire set of computations has to be repeated many times.

In this paper we present a set of absorbing boundary conditions that are based on paraxial approximations (PA) of the scalar and elastic wave equations. A discussion of these types of boundary conditions based on pseudo-differential operators, for a general class of differential equations, can be found in Engquist and Majda (1977). The chief feature of the PA that we will exploit is that the outward-moving wave field can be separated from the inward-moving one. Along the boundary, then, the PA can be used to model only the outward-moving energy and hence reduce the reflections. The boundary conditions that we present are stable and computationally efficient in that they require about the same amount of work per mesh point for finite difference applications as does the full wave equation.

In the first part of this paper, some paraxial approximations to the scalar and elastic wave equations are presented. In the second part, the PA are used as absorbing boundary conditions and expressions for the effective reflection coefficients along the boundary are given. Some numerical examples are presented in the final section.

Paraxial Approximations of the Wave Equation

Paraxial approximations of the scalar wave equation have been extensively developed by Claerbout (1970, 1976), and Claerbout and Johnson (1971), and in the first part of this section we present a brief review of that work. In the second part we develop paraxial approximations for the elastic wave equation.

The two-dimensional scalar wave equation

$$P_{xx} + P_{zz} = v^{-2}P_{tt}, \tag{1}$$

is usually considered for modeling purposes to be initial valued in time. The stability of the equation for time extrapolation is ensured by the fact that in its dispersion relation

$$\omega = v(k_x^2 + k_z^2)^{1/2}, \tag{2}$$

the frequency ω is a real function of the spatial wave numbers k_x and k_z.

If we now consider spatial extrapolation of (1) (say, in the z-direction), the appropriate form of the dispersion relation would be

$$k_z = \pm(\omega/v)[1 - (v^2k_x^2/\omega^2)]^{1/2}. \tag{3}$$

Clearly there are stability problems when $|vk_x/\omega| > 1$ (evanescent waves), because k_z becomes imaginary. It is therefore necessary to modify the wave equation in such a way as to eliminate the evanescent components of the solution. A relatively simple way of accomplishing this is to restrict the range of solutions to those waves that are traveling within a cone of the z-axis (paraxial waves). Note that the $\pm$ sign in equation (3) is for wave fields moving in opposite directions in z, and we will model these fields separately.

To form the paraxial approximation of (1), we expand the square-root operator of (3) as a rational approximation about small vk_x/ω. Three such approximations [for the + sign of equation (3)] are

$$\text{A1:}\quad vk_z/\omega = 1 + 0(|vk_x/\omega|^2), \tag{4}$$

$$\text{A2:}\quad vk_z/\omega = 1 - \frac{1}{2}(vk_x/\omega)^2 + 0(|vk_x/\omega|^4), \tag{5}$$

$$\text{A3:}\quad \frac{vk_z}{\omega} = \frac{1 - \frac{3}{4}(vk_x/\omega)^2}{1 - \frac{1}{4}(vk_x/\omega)^2} + 0(|vk_x/\omega|^6). \tag{6}$$

A general order expansion, which leads to stable differencing schemes, can be found by the recursion relation for a Padé series approximation to a square root (Francis Muir, personal communication)

$$a_j = 1 - \frac{(vk_x/\omega)^2}{1 + a_{j-1}} + 0(|vk_x/\omega|^{2j}), \qquad a_1 = 1, \tag{7}$$

where the jth paraxial approximation is given by $vk_z/\omega = a_j$. The dispersion relations A1, A2, A3, and the dispersion relation of the full wave equation are shown in Figure 1.

The error term in the expansions indicates that the approximations are valid for

waves traveling within a cone of the z-axis. A similar set of equations can be derived for the minus sign of equation (3). In this way, the incoming and outgoing wave fields are separated by the paraxial approximation. It is interesting to note that higher-order approximations based on Taylor series expansions of the square root in equation (3) lead to unstable differencing schemes (Engquist and Majda, 1977).

In their differential form, equations (4 to 6) appear as

$$\text{A1: } P_z + (1/v)P_t = 0, \tag{8}$$

$$\text{A2: } P_{zt} + (1/v)P_{tt} - (v/2)P_{xx} = 0, \tag{9}$$

$$\text{A3: } P_{ztt} - (v^2/4)P_{zxx} + (1/v)P_{ttt} - (3v/4)P_{txx} = 0. \tag{10}$$

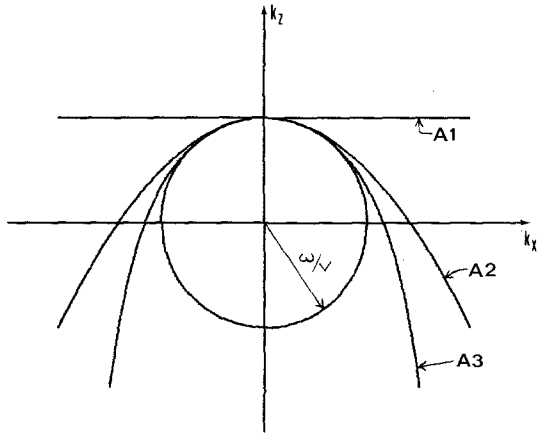

FIG. 1. Dispersion relations for the scalar case. The curves A1, A2, and A3 are the dispersion relations of the paraxial approximations of the scalar wave equation (the circle).

Note that equations (8 to 10) are somewhat different from those of Claerbout (1976) because he uses a retarded time coordinate system which cannot be used here.

Paraxial approximations for the elastic wave equation analogous to those of the scalar wave equation can also be found. We cannot, however, perform the analysis by considering expansions of the dispersion relation because the differential equations for vector fields are not uniquely specified from their dispersion relations. Instead, we use the scalar case to provide a hint as to the general form of the paraxial approximation and fit the coefficients by matching to the full elastic wave equation.

We write the elastic wave equation for a homogeneous, isotropic medium in the form

$$\underline{u}_{tt} = D_1\underline{u}_{xx} + H\underline{u}_{xz} + D_2\underline{u}_{zz}, \tag{11}$$

where

$$\underline{u} = \begin{pmatrix} u \\ v \end{pmatrix} = \begin{pmatrix} \text{horizontal displacement field} \\ \text{vertical displacement field} \end{pmatrix},$$

$$D_1 = \begin{pmatrix} \alpha^2 & 0 \\ 0 & \beta^2 \end{pmatrix}; \qquad D_2 = \begin{pmatrix} \beta^2 & 0 \\ 0 & \alpha^2 \end{pmatrix}; \qquad H = (\alpha^2 - \beta^2) \cdot \begin{pmatrix} 0 & 1 \\ 1 & 0 \end{pmatrix},$$

and α and β are the compressional and shear velocities, respectively. The Fourier transform of this equation is

$$[I - D_1(k_z/\omega)^2 - H(k_x/\omega)(k_z/\omega) - D_2(k_x/\omega)^2]\tilde{\underline{u}}(\omega, k_x, k_z) = 0. \quad (12)$$

We now consider two forms of the paraxial approximation

$$\text{A1: } \underline{u}_z + B_1\underline{u}_t = 0, \quad (13)$$

and

$$\text{A2: } \underline{u}_{tz} + C_1\underline{u}_{tt} + C_2\underline{u}_{tx} + C_3\underline{u}_{xx} = 0. \quad (14)$$

In A2 the C_2 term describes the coupling of u and w. The Fourier transforms of these approximations are

$$\text{A1: } [I(k_z/\omega) - B_1]\tilde{\underline{u}}(\omega, k_x, k_z) = 0, \quad (15)$$

and

$$\text{A2: } [I(k_z/\omega) - C_1 + C_2(k_x/\omega) - C_3(k_x/\omega)^2]\tilde{\underline{u}}(\omega, k_x, k_z) = 0. \quad (16)$$

In equations (15) and (16), the (k_z/ω) term may be isolated and substituted in (12) to determine the coefficient matrices in (13) and (14). The results are

$$B_1 = C_1 = \begin{pmatrix} 1/\beta & 0 \\ 0 & 1/\alpha \end{pmatrix},$$

$$C_2 = (\beta - \alpha)\begin{pmatrix} 0 & 1/\beta \\ 1/\alpha & 0 \end{pmatrix},$$

$$C_3 = \frac{1}{2}\begin{pmatrix} \beta - 2\alpha & 0 \\ 0 & \alpha - 2\beta \end{pmatrix}.$$

The error terms for the A1 and A2 approximations are $0(|k_x/\omega|)$ and $0(|k_x/\omega|^3)$, respectively.

In Figure 2 the dispersion relations for (13) and (14) are presented. The dispersion relations in this case are the loci of zeros of the determinant of the square-bracketed quantities in (15) and (16). The fact that there are two curves for each approximation indicates that they decouple into compressional and shear motions, as does the full wave equation. For the approximation A2, the shape of the dispersion curves depends on the ratio of α and β, and in Figure 2 an α/β ratio of $\sqrt{3}$ is used. In general, the larger the velocity ratio becomes, the poorer the approximation for shear waves.

In Figure 2, we have also presented the dispersion relation for the viscous boundaries of Lysmer and Kuhlemeyer (1969). The curve is a hyperbola that is independent of velocity ratio, and it indicates that the viscous boundaries will model shear waves less accurately than either the A1 or A2 approximations.

Absorbing Boundary Conditions

The dispersion curves presented in the previous section indicate that the paraxial approximations can be used to model both elastic and scalar waves moving in one

general direction and to discriminate against waves moving in the opposite direction. To absorb incident energy along a given boundary, then, we can use the paraxial approximation that models only energy moving outward from the interior of the grid

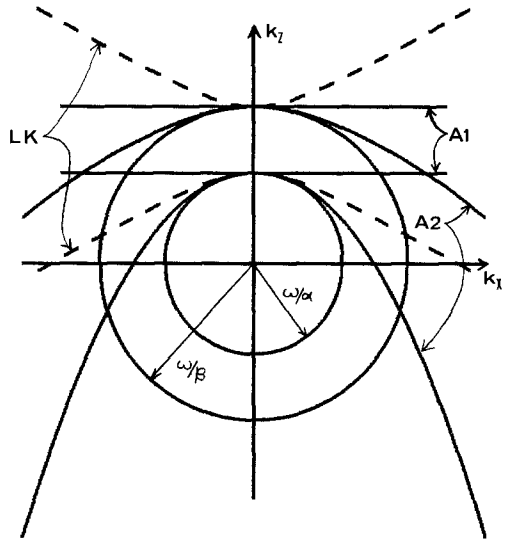

FIG. 2. Dispersion relations for the elastic case. The curves A1 and A2 are the dispersion relations of the paraxial approximations of the elastic wave equation (the circles). For each approximation there are two curves: that approximating the larger circle is for shear waves while the other is for compressional waves. The dashed curves (labeled LK) are the dispersion curves of the viscous boundary conditions of Lysmer and Kuhlemeyer (1969).

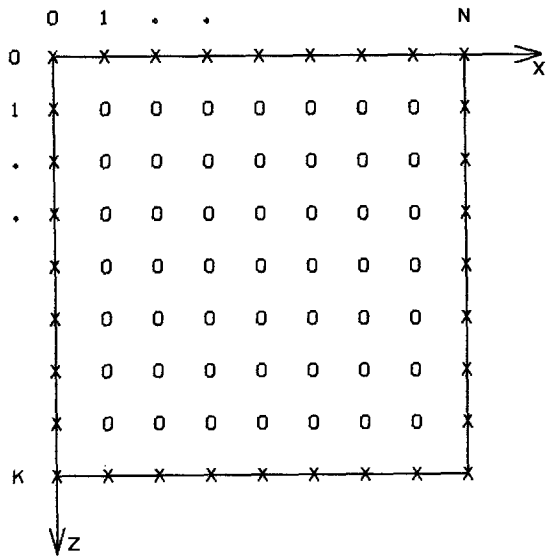

FIG. 3. Computational grid.

toward that boundary. All of the approximations presented in the previous section modeled waves moving in the positive z-direction. Hence, on the grid shown in Figure 3, they would be suitable for absorbing boundary conditions along the bottom edge. For the top edge, we would use the paraxial approximations which correspond to taking the negative sign on the radical of equation (3). In this case, the dispersion

relations would be approximating the lower half of the semicircle. The boundary conditions for the sides are found by interchanging x and z in the two cases above.

To clarify the method we shall present the scheme used for the numerical examples in some detail. For each time step:

1. We solved all interior points (marked "o" in Figure 3) with an explicit finite difference form of the full wave equation [equations (1) or (11)]. See Kelly *et al.* (1976) for the difference formulas.

2. We used the appropriate paraxial approximation to extrapolate spatially the interior solution one mesh row outward to fill in the boundary row (marked "x" in Figure 3). Since all of the paraxial approximations are first order in the spatial extrapolation direction, only the nearest interior row is needed for each boundary. The actual difference schemes are presented in the Appendix.

The effectiveness of the various absorbing boundary conditions given here can be gauged by comparing their effective reflection coefficients at the boundaries. For the scalar wave equation, consider an incident plane wave traveling in the positive z-direction

$$P_I = \exp\,(ik_x x + ik_z z - i\omega t),$$

which initiates a reflection from the bottom boundary of the form

$$P_R = r \exp\,(ik_x x - ik_z z - i\omega t),$$

where r is the effective reflection coefficient. Locally near the boundary, the wave field $P_I + P_R$ will satisfy both the boundary condition and the interior equation. Applying the boundary condition A2, for example, we obtain

$$k_z \omega(P_I - rP_R) - \left(\frac{\omega^2}{v} - \frac{v}{2} k_x^2\right)(P_I + rP_R) = 0.$$

Solving for r and evaluating at the boundary, we obtain

$$r = -\frac{1 - \frac{1}{2}(vk_x/\omega)^2 - (vk_z/\omega)}{1 - \frac{1}{2}(vk_x/\omega)^2 + (vk_z/\omega)}.$$

By noting that from the interior equation $(vk_x/\omega)^2 = 1 - (vk_z/\omega)^2$ and identifying vk_z/ω as $\cos\theta$ where θ is the angle of incidence measured from the normal to the boundary, we can write the reflection coefficient as

$$r(\theta) = -[(1 - \cos\theta)/(1 + \cos\theta)]^2.$$

This expression may be generalized for the A_j boundary condition to

$$r_j(\theta) = -[(1 - \cos\theta)/(1 + \cos\theta)]^j.$$

In Figure 4, the reflection coefficients for A1, A2, and A3 are plotted. It should be noted that angles where $r(\theta)$ is large correspond to waves traveling almost parallel to the boundary. They would therefore likely strike another absorbing boundary before interacting with the solution at the center of the grid. A measure of the energy

radiated toward the center of the grid would be

$$[r_j(\theta) \sin \theta]^2.$$

To find the effective reflection coefficients for elastic waves, we assume plane-wave potential solutions of the form

$$\Phi = \Phi_0 \exp i(\omega/\alpha)(l_\alpha x + n_\alpha z) + r_P \exp i(\omega/\alpha)(l_\alpha x - n_\alpha z),$$

$$\Psi = \Psi_0 \exp i(\omega/\beta)(l_\beta x + n_\beta a) + r_S \exp i(\omega/\beta)(l_\beta x - n_\beta z),$$

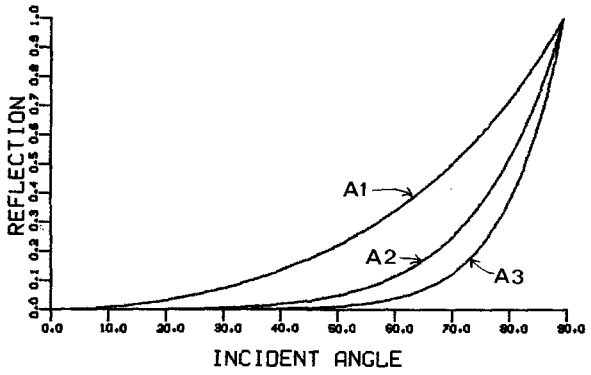

FIG. 4. Reflection coefficients for the scalar case. The curves are the effective reflection coefficients for the scalar absorbing boundary conditions A1, A2, and A3.

where l_α, n_α, l_β, and n_β are the direction cosines of the wave front. For incident compressional waves, $\Phi_0 = 1$ and $\Psi_0 = 0$, and for incident shear waves $\Phi_0 = 0$ and $\Psi_0 = 1$. The displacement fields are found by the transformation

$$u = \Phi_x + \Psi_z,$$

$$w = \Phi_z - \Psi_x.$$

The expressions for the horizontal and vertical displacements are substituted into the time-transformed form of the boundary conditions A1 and A2, and the reflection coefficients r_P and r_S are determined. In Figures 5 and 6, we show the reflection coefficients for the boundary conditions A1 and A2, respectively. The abrupt changes in reflection coefficients (marked by arrows) for incident shear waves are due to the formation of a pseudo-head wave along the boundary. These waves do not in practice interfere with the computation at the center of the grid.

In Figure 7, the effective reflection coefficients for the viscous boundaries (Lysmer and Kuhlemeyer, 1969) are shown.

In the discussion above on absorbing boundary conditions, we have assumed that there is no *a priori* information on wave direction at the boundaries. In some studies, such as monochromatic surface wave studies, this information does exist and can be used to "tune" the boundary condition. In this case the paraxial approximations are expanded about the preferred wave direction rather than normal incidence. In Figures 1 and 2, this amounts to a rotation of the dispersion curves about the origin, so that

the best fit to the circles occurs at the preferred propagation angle. In the numerical examples that follow, the corner points of the mesh were made transparent by a 45° rotation of the A1 boundary conditions. Thus all waves traveling directly into the corners are perfectly absorbed.

Numerical Examples

To illustrate the effectiveness of the boundary conditions, we present three examples. In each case, the computations were done with the usual Neumann (zero-

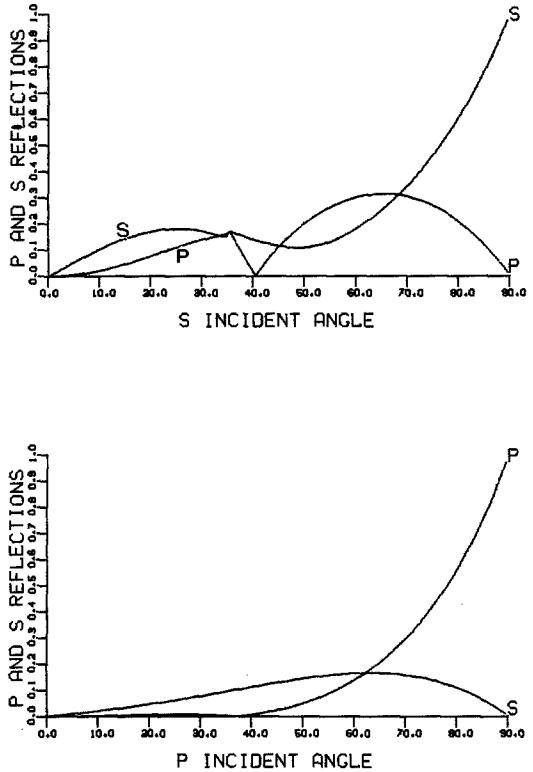

Fig. 5. Reflection coefficients for the A1 elastic boundary condition. In the top panel shear (S) and compressional (P) reflections are shown for an incident S wave of unit strength, while in the bottom panel P and S reflections are shown for incident P waves. This wave does not penetrate into the region of computation.

slope) boundary conditions and with the A2 absorbing boundary conditions. A 40 by 40 grid was used with the mesh spacing chosen to make the explicit differencing scheme for the interior solution stable.

The first example, Figure 8, is a circularly spreading scalar wave. The Neumann conditions make the boundary act as a perfect reflector, but the absorbing boundary conditions allow the wave to pass through the grid perimeter.

The second example, Figure 9, is a circular compressional elastic wave. Both the horizontal and vertical wave fields are depicted with "black" representing positive amplitudes and "white" representing negative amplitudes. A velocity ratio of $\alpha/\beta = \sqrt{3}$ was used.

The final example, Figure 10, is a circular shear wave, and again $\alpha/\beta = \sqrt{3}$ was used.

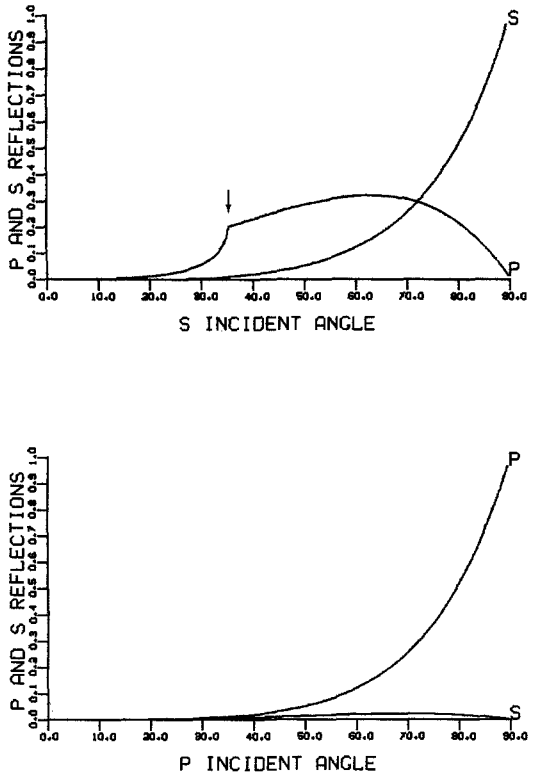

FIG. 6. Reflection coefficients for the A2 elastic boundary condition. See Figure 5 for details. In this case, the S reflection for incident P is much more diminished than in the A1 case, which is important because it reflects more closely to the normal than does the P wave. For incident S waves, both P and S reflections are smaller than with the A1 case.

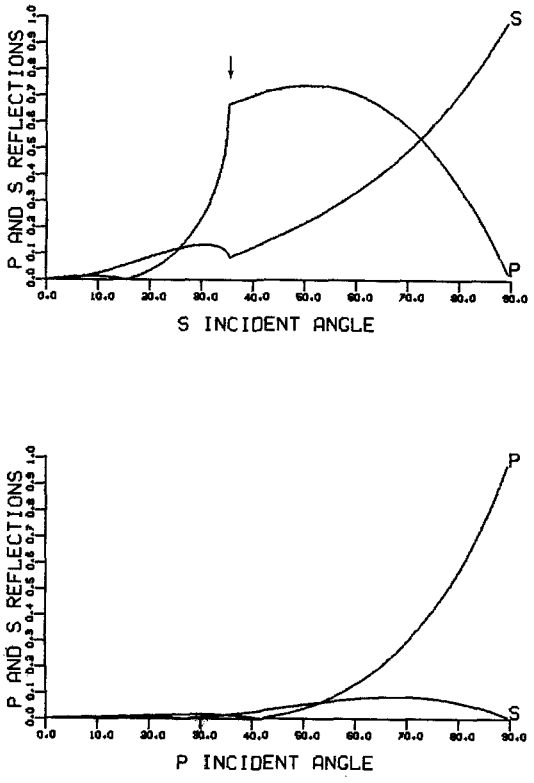

FIG. 7. Reflection coefficients of the viscous boundary condition for the elastic equation. See Figure 5 for details. For both P and S incident waves, the amplitude of the reflected waves is larger than with the A2 boundary conditions.

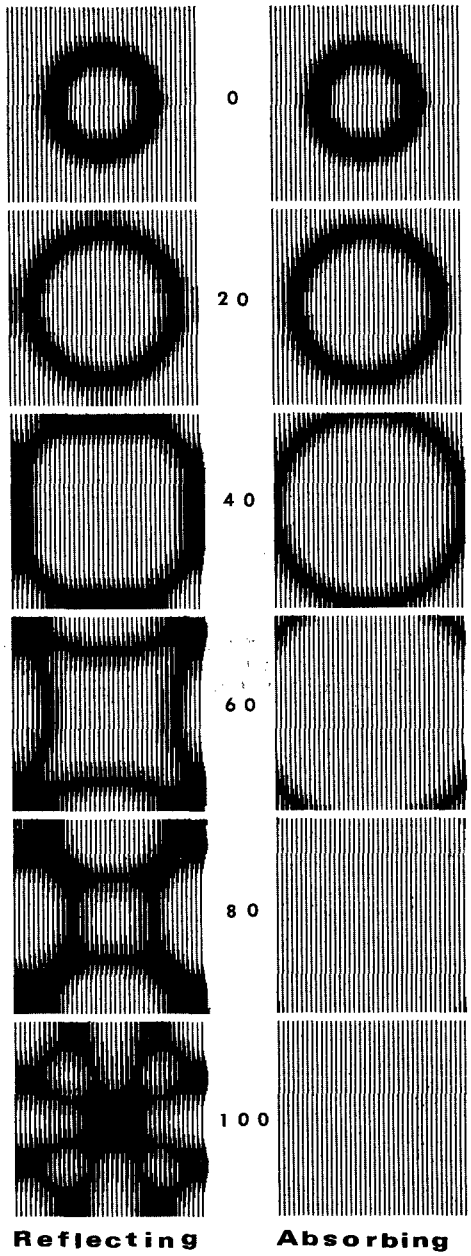

FIG. 8

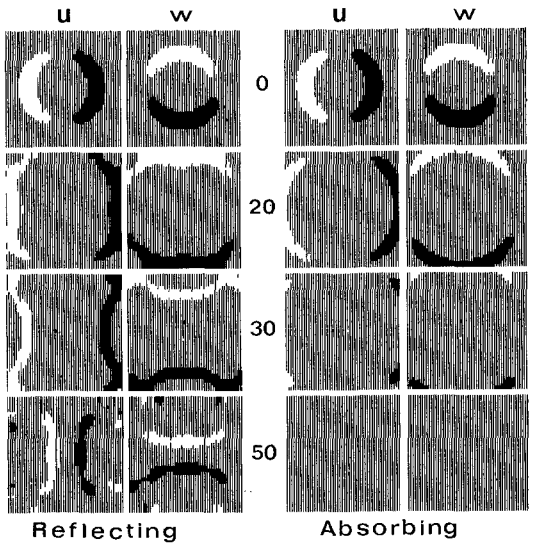

FIG. 9

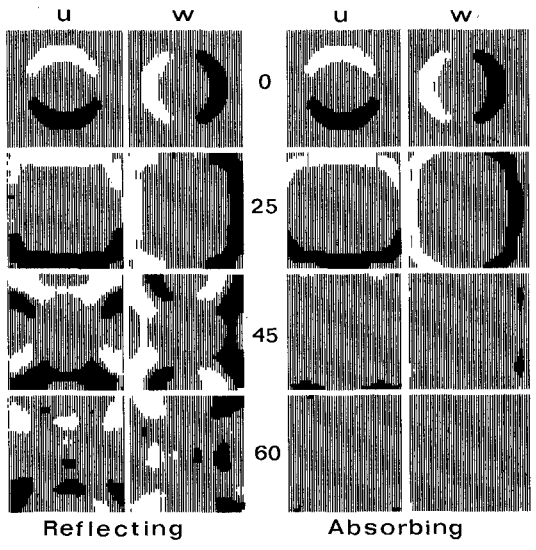

FIG. 10

FIG. 8. Reflecting and absorbing boundary conditions for an expanding circular scalar wave. The absorbing boundary condition was applied with the A2 scalar differencing scheme given in the Appendix. The numbers refer to the time step index.

FIG. 9. Reflecting and absorbing boundary conditions for an expanding compressional wave. The absorbing boundary condition was applied with the A2 elastic difference scheme given in the Appendix. The horizontal and vertical displacements are denoted by U and W, respectively. The numbers are the time index.

FIG. 10. Reflecting and absorbing boundary conditions for an expanding shear wave. Refer to Figure 9.

Conclusions

A set of boundary conditions for scalar and elastic waves that reduce artificial reflections has been presented. The boundary conditions are essentially paraxial approximations of the scalar and elastic wave equations. The advantages of these boundary conditions are, first, that they absorb energy over a wide range of incident angles, and, second, that they are computationally inexpensive and simple to apply.

By using the paraxial approximation to derive absorbing boundary conditions, we have presented a general approach for differential equations of various types. The accuracy of these boundary conditions can be increased by simply taking higher-order paraxial approximations.

Acknowledgments

We thank Professor Jon Claerbout for his valuable suggestions, and the sponsors of the Stanford Exploration Project for their financial support.

References

Claerbout, J. F. (1970). Coarse grid calculations of waves in inhomogeneous media with application to delineation of complicated seismic structure, *Geophysics* **35**, 407–418.

Claerbout, J. F. (1976). *Fundamentals of Geophysical Data Processing*, McGraw-Hill, New York, 163–226.

Claerbout, J. F. and A. G. Johnson (1971). Extrapolation of time dependent waveforms along their path of propagation, *Geophys. J.* **26**, 285–295.

Engquist, B. and A. Majda (1977). Absorbing boundary conditions for the numerical simulation of waves, *Math. Comp.* (in press).

Kelly, K. R., R. W. Ward, S. Treitel, and R. M. Alford (1976). Synthetic seismograms: a finite-difference approach, *Geophysics* **41**, 2–27.

Lysmer, J. and R. L. Kuhlemeyer (1969). Finite dynamic model for infinite media, *J. Eng. Mech. Div., ASCE* **95** EM4, 859–877.

Smith, W. D. (1974). A non-reflecting plane boundary for wave propagation problems, *J. Comp. Phys.* **15**, 492–503.

Department of Geophysics
Stanford University
Stanford, California (R.C.)

Department of Computer Sciences
Uppsala University
Uppsala, Sweden (B.E.)

Manuscript received May 11, 1977

Appendix

The finite difference formulas for the A2 scalar absorbing boundary condition (equation 9) are given below. Refer to Figure 3 for the computational grid.

Top ($k = 0$)

$$D_+^z D_0^t P_{j,0}^n - (\tfrac{1}{2}v) D_+^t D_-^t (P_{j,0}^n + P_{j,1}^n) + (v/4) D_+^x D_-^x (P_{j+1,1}^n + P_{j-1,0}^n) = 0.$$

Bottom ($k = K$)

$$D_-^z D_0^t P_{j,K}^n + (\tfrac{1}{2}v) D_+^t D_-^t (P_{j,K}^n + P_{j,K-1}^n) - (v/4) D_+^x D_-^x (P_{j+1,K-1}^n + P_{j-1,K}^n) = 0.$$

Left side ($n = 0$)

$$D_+^z D_0^t P_{j,k}^0 - (\tfrac{1}{2}v) D_+^t D_-^t (P_{j,k}^0 + P_{j,k}^1) + (v/4) D_+^z D_-^z (P_{j+1,k}^1 + P_{j-1,k}^0) = 0$$

Right side ($n = N$)

$$D_-^z D_0^t P_{j,k}^N + (\tfrac{1}{2}v) D_+^t D_-^t (P_{j,k}^N + P_{j,k}^{N-1}) - (v/4) D_+^z D_-^z (P_{j+1,k}^{N-1} + P_{j-1,k}^N) = 0.$$

Here

$$P_{j,k}^n \approx P(t_j, z_k, x_n),$$

and D_+^q, D_-^q, and D_0^q are, respectively, the forward, backward, and center difference operators with respect to the variable q; i.e., $D_+^z P_{j,k}^n = (P_{j,k+1}^n - P_{j,k}^n)/\Delta z$.

For the second-order elastic boundary conditions (equation 14), the difference schemes are:

Top ($k = 0$)

$$D_+^z D_0^t \underline{u}_{j,0}^n - (\tfrac{1}{2})C_1 D_+^t D_-^t(\underline{u}_{j,0}^0 + \underline{u}_{j,1}^n) - (\tfrac{1}{2})C_2 D_+^t D_0^x(\underline{u}_{j-1,0}^n + \underline{u}_{j,1}^n)$$
$$- (\tfrac{1}{2})C_3 D_+^x D_-^x(\underline{u}_{j-1,0}^n + \underline{u}_{j+1,1}^n) = 0.$$

Bottom ($k = K$)

$$D_-^z D_0^t \underline{u}_{j,K}^n + (\tfrac{1}{2})C_1 D_+^t D_-^t(\underline{u}_{j,K}^n + \underline{u}_{j,K-1}^n) + (\tfrac{1}{2})C_2 D_+^t D_0^x(\underline{u}_{j-1,K}^n + \underline{u}_{j,K-1}^n)$$
$$+ (\tfrac{1}{2})C_3 D_+^x D_-^x(\underline{u}_{j-1,K}^n + \underline{u}_{j+1,K-1}^n) = 0.$$

Left side ($n = 0$):

$$D_+^x D_0^t \underline{u}_{j,k}^0 - (\tfrac{1}{2})C_1 D_+^t D_-^t(\underline{u}_{j,k}^0 + \underline{u}_{j,k}^1) - (\tfrac{1}{2})C_2 D_+^t D_0^z(\underline{u}_{j-1,k}^0 + \underline{u}_{j,k}^1)$$
$$- (\tfrac{1}{2})C_3 D_+^z D_-^z(\underline{u}_{j-1,k}^0 + \underline{u}_{j+1,k}^1) = 0.$$

Right side ($n = N$)

$$D_-^x D_0^t \underline{u}_{j,k}^N + (\tfrac{1}{2})C_1 D_+^t D_-^t(\underline{u}_{j,k}^N + \underline{u}_{j,k}^{N-1}) + (\tfrac{1}{2})C_2 D_+^t D_0^z(\underline{u}_{j-1,k}^N + \underline{u}_{j,k}^{N-1})$$
$$+ (\tfrac{1}{2})C_3 D_+^z D_-^z(\underline{u}_{j-1,k}^N + \underline{u}_{j+1,k}^{N-1}) = 0.$$

Here,

$$\underline{u}_{j,k}^n \approx \underline{U}(t_j, z_k, x_n).$$

The three points along the boundary in each corner are computed with a 45° rotation of the A1 boundary condition. For example, the differential and difference boundary condition formulas for the lower right-hand corner are:

scalar waves

$$P_z + P_x + (\sqrt{2}/v)P_t = 0,$$

$$[D_-^z + D_-^x + (\sqrt{2}/v)D_-^t]P_{j,k}^n = 0, \quad (k, n) = (K, N-1), (K-1, N), (K, N);$$

elastic waves

$$\underline{u}_z + \underline{u}_x + M\underline{u}_t = 0,$$

$$(D_-^z + D_-^x + MD_-^t)\underline{u}_{j,k}^n = 0 \qquad (k, n) = (K, N-1), (K-1, N), (K, N);$$

where

$$M = \frac{1}{\sqrt{2}}\begin{pmatrix} (1/\beta) + (1/\alpha) & (1/\beta) - (1/\alpha) \\ (1/\beta) - (1/\alpha) & (1/\beta) + (1/\alpha) \end{pmatrix}.$$